Mapping of spatiotemporal heterogeneous particle dynamics in living cells

Michael H. G. Duits, Yixuan Li, Siva A. Vanapalli, and Frieder Mugele
Physics of Complex Fluids group, Faculty of Science and Technology and MESA+ Institute for Nanotechnology, University of Twente, P.O. Box 217, 7500 AE Enschede, The Netherlands

(Received 21 November 2008; revised manuscript received 17 February 2009; published 13 May 2009)

Colloidal particles embedded in the cytoplasm of living mammalian cells have been found to display remarkable heterogeneity in their amplitude of motion. However, consensus on the significance and origin of this phenomenon is still lacking. We conducted experiments on Hmec-1 cells loaded with about 100 particles to reveal the intracellular particle dynamics as a function of both location and time. Central quantity in our analysis is the amplitude (A) of the individual mean-squared displacement (iMSD), averaged over a short time. Histograms of A were measured, (1) over all particles present at the same time and (2) for individual particles as a function of time. Both distributions showed significant broadening compared to particles in Newtonian liquid, indicating that the particle dynamics varies with both location and time. However, no systematic dependence of A on intracellular location was found. Both the (strong) spatial and (weak) temporal variations were further analyzed by correlation functions of A. Spatial cross correlations were rather weak down to interparticle distances of 1 μm, suggesting that the precise intracellular probe distribution is not crucial for observing a dynamic behavior that is representative for the whole cell. Temporal correlations of A decayed at $\sim$10 s, possibly suggesting an intracellular reorganization at this time scale. These findings imply (1) that both individual particle dynamics and the ensemble averaged behavior in a given cell can be measured if there are enough particles per cell and (2) that the amplitude and power-law exponent of iMSDs can be used to reveal local dynamics. We illustrate this by showing how superdiffusive and subdiffusive behaviors may be hidden under an apparently diffusive global dynamics.

DOI: 10.1103/PhysRevE.79.051910 PACS number(s): 87.16.dm, 87.16.Ln, 87.16.dj, 87.85.jc

I. INTRODUCTION

Recent literature has witnessed a strong increase in the use of colloidal particles as local tracers of dynamic processes in soft materials [1,2]. What makes these particles so suitable is that they are both small enough to show Brownian motion and large enough to probe the deformations of the soft material network. Then the motion of each particle is driven by mechanical excitations from surrounding molecules on one hand and damped by its viscoelastic microenvironment on the other. Conversely, information about these forces can also be obtained by analyzing the statistics of particle motion. A good example is the study of passive engineering materials with particle tracking microrheology (PTM); here the assumptions that all particle motions are driven by thermal collisions and that the fluctuation-dissipation theorem (FDT) applies are used to calculate viscoelastic properties of the material from the mean-squared displacement (MSD) of the particles as a function of lag time [3].

Alternatively, also the interior (i.e., cytoplasm) of living biological cells has been studied with the methods from PTM [4–19]. Measuring the statistical motions of (endogenous or microinjected) particles provides a direct way to study intracellular mechanics at (sub)micron length scales. Yet there are also certain challenges involved. In the earliest PTM studies on soft biological matter it was recognized that besides the size, also the chemistry of the probe can have strong influence on the MSD functions obtained [9,20,21]. More recently, also contributions of adenosine triphosphate (ATP) dependent processes to particle dynamics have been identified [16,18,22]. Together, these studies have resulted in a general consensus that the FDT is violated and that intracellular particle MSDs can reflect thermal or ATP-dependent driving forces, viscoelastic damping, or combinations thereof.

Which information can be obtained from MSDs measured inside living cells then depends on the experimental conditions and on the time and/or length scales addressed. Restricting the analysis to short lag times [22] and suppressing active motion by ATP depletion [12] are possibly strategies to measure viscoelastic properties of the cytoplasm. Alternatively, in cases where probes cannot be assumed to be chemically inert and driven by thermal collisions, their MSDs can still provide unique information. For example, probes attached to specific intracellular structures (such as the actin network or microtubules) can reveal structural or dynamic changes in these networks.

An additional aspect encountered in intracellular studies is that the dynamic behavior varies from particle to particle. Considering the complexity and structural heterogeneity of living cells, this finding is not surprising, but it also raises the question of how to deal with this heterogeneous dynamics. Most studies have been aimed at measuring a behavior representative for the whole cell. For single large (4 μm) beads [12] this was achieved by temporal averaging, while in studies with several small (100–500 nm) particles distributed over the cell [6,7,10,13], both spatial and temporal averaging were used to obtain an overall MSD. However, that obtaining such a representative MSD from just a few particles per cell is far from trivial is also clear, considering that the MSD amplitude sometimes varies over more than an order of magnitude [4,5,9,14,15].

Relatively few studies have been aimed at studying these heterogeneities themselves. Using multiple particle tracking

[one-point microrheology (1PMR)], Heidemann and Wirtz [4] and Kole *et al.* [5] reported cytoplasmic stiffening near the leading edges of migrating Swiss 3T3 fibroblasts, in agreement with the required local functionality of the cell. In another study, nonmigrating fibroblasts were reported to have a mechanical compliance that depended on the distance from the nucleus. This was described as an intrinsic mechanical heterogeneity [9]. Alternatively, other researchers addressed the aspect of spatial heterogeneity via both one-point microrheology and two-point microrheology (2PMR) [14,15,23]. Since the D_{rr} correlator was found to scale with interprobe distance r as $\sim 1/r$ for $2<r<8$ μm (as expected for a homogeneous medium), Van Citters *et al.* [15] concluded that gross-scale mechanical heterogeneity was absent in TC7 epithelial cells. However experiments with a single large bead per cell had shown large amplitude variations from cell to cell [14,15]. These were attributed to variations in (adhesive) contact between probe and matrix. In a study by Bursac *et al.* [18], a relation between binding state and MSD behavior was found for externally attached beads. Thus in literature, different physical origins have been suggested for the spatially heterogeneous dynamics found in cells: mechanical heterogeneity [4,5] and a variability in tracer-cytoskeleton contacts [15,18].

The temporal aspect of heterogeneity has been addressed even less even though the potential role hereof has been pointed out [14,19,24,25]. A clear example is the intermittent dynamics [19] displayed by particles that are for short episodes actively transported via linkage to a motor protein but otherwise free to diffuse. Also less conspicuous temporal variations can occur. For example, cytoskeleton remodeling can expose a particle to a new microenvironment, or a change in the binding state between probe and matrix can cause a change in dynamics. The consequences of such events on time averaged MSDs have hardly been explored so far.

Thus a lot is still missing in our understanding of the spatiotemporal heterogeneity of intracellular particle dynamics. This lack of knowledge can seriously obstruct interpretation of intracellular particle tracking experiments in several respects. First it raises the question, under which conditions a "blind averaging" over intracellular MSDs will produce a total MSD that is representative for the whole cell. Second, due to temporal fluctuations, also the analysis of the individual MSDs may become obscured. By default one might assume that during the time span in which particles are tracked, the dynamic behavior does not change. But if, for example, a particle switches intermittently between two simple dynamic behaviors, and the integration time over the trajectory is too long, then these individual behaviors will be washed out, producing an iMSD that is hard to interpret. And third, a lack of knowledge on the phenomenology of spatiotemporal heterogeneity also obstructs finding its physical origin(s).

In this paper we present a detailed study of the spatial and temporal heterogeneities in the dynamics of intracellular particles. Two goals were pursued. First, we wanted to assess the relative importance of spatial and temporal heterogeneities in a chosen type of cell and measure the characteristic length and time scales over which the dynamic behavior of individual particles can change. And second, we wanted to explore tools to characterize mechanically heterogeneous materials in general. Besides biological cells also many engineering materials display spatial or spatiotemporal heterogeneity. Examples are associating polymer solutions [26], gels [24,27,28], protein suspensions [29], gelled and jammed colloids [1,30], and two phase materials [31].

For the present work we chose to analyze the dynamics of endogenous granules (EGs) in living Hmec-1 cells [also artificially introduced latex particles called ballistically injected particles (BIPs) will be considered, albeit in less detail]. This intracellular probe has been studied before [10,12,13,32,33] and is known to display heterogeneous dynamics when studied with 1PMR [10]. We will use the iMSD amplitude measured at the shortest lag time as the central quantity. Its dependence on location and time will be studied via correlation functions and variance analysis. To achieve sufficient accuracy we analyze a large data set containing $\approx 10^5$ trajectories, of which a significant fraction has long duration (>1000 time steps). Significance of the measured heterogeneities will be assessed by comparing the results to reference cases: experiments in viscous liquid and computer simulations for particles showing Brownian motion.

Importantly, we will conclude that our particles have distinguishable dynamics within the 150 s time scale of our experiments. Building on this outcome, we then examine the distributions in MSD amplitude and power-law exponent. We will show that both quantities show a significant distribution, for both EGs and BIPs. The broad range of power-law exponents indicates that not only the motion amplitude but also the qualitative dynamic behavior of the same kind of particles present inside the same cell can be very different.

This paper is further organized as follows. In Sec. II we describe the technical details of the experiments and the computer simulations. In Sec. III we develop a number of statistical tools to analyze MSDs and illustrate some of their properties using numerically simulated MSD traces. In Sec. IV we will present a quantitative analysis of the spatial and temporal heterogeneities displayed by EGs in confluent Hmec-1 cells. Based on these findings, we present in Sec. V an extended analysis covering also the different types of dynamic behavior of EGs and BIPs in individual Hmec-1 cells. Conclusions will be drawn in Sec. VI.

II. EXPERIMENTS

A. Cell culture

Human microvascular endothelial cells (Hmec-1) (TNO, Leiden, The Netherlands) at 25–30 passages were cultured at 37 °C in a humidified 5% CO_2 environment in endothelial cell growth medium containing hydrocortisone, hFGF, R3-IGF-1, ascorbic acid, hEGF, gentamicin, heparin, and 2% fetal bovine serum (EGM-2, Lonza, Basel, Switzerland). Cells were plated on a delta T culture dish (Bioptechs, Butler, PA, USA) precoated with fibronectin (100 μg/ml solution) and mounted on an inverted microscope before experiments. The dish bottom contains a thin ITO layer, whose temperature was controlled via a heating system (Bioptechs).

A heated lid was used to seal the culture dish, and 5% CO_2 was supplied continuously.

B. Probe types

We used two intracellular probes—EGs and ballistically injected particles (BIPs). The EGs, having a mean size of ≈ 0.5 μm, were confirmed to be mainly lipid droplets and some mitochondria by staining with Nile red and rhodamine dyes, respectively. These granules appear as dark objects under phase contrast microscopy. For the BIPs we chose fluorescently labeled carboxylated polystyrene spheres with diameter of 0.2 μm (invitrogen). These particles were introduced via ballistic injection as described by Panorchan *et al.* [6] and visualized by illuminating with an Ar laser ($\lambda = 488$ nm).

C. Intracellular particle tracking

Probe particles were visualized using a Nikon Eclipse TE300 inverted microscope coupled to a confocal module (UltraView LCI 10, Perkin Elmer, Cambridge, U.K.). EGs and BIPs were imaged under phase contrast and fluorescence mode, respectively, using a 100× (NA 1.3) objective. Images were recorded with a 12-bit charge coupled device (CCD) camera (Hamamatsu IEEE 1394 C4742–95–12 ERG). The unit exposure time was set to 60 ms, and the spatial resolution corresponding to the images was 0.13 μm per pixel. Probe motion was studied in individual cells (both under confluent and nonconfluent conditions) that contained a large number of particles: typically 40 for BIPs and 80 for EGs. To obtain enough observations for our statistical analysis, we recorded in between 10 and 41 movies (of 2500 frames each) per cell. Statistical analyses (of correlations and variances, see Sec. III) were always performed on a single cell. The time-dependent locations of the particles were obtained using the available code [34], originally based on the paper of Crocker and Grier [35] and written and extended in interactive data language (IDL). The error in our measurement of the particle displacements was 10 nm.

D. Computer simulations

Brownian dynamics simulations were performed to generate reference data for use in interpretation. The case of uniformly sized particles in a Newtonian liquid was mimicked by spreading typically 200 particles over an XY area and subsequently letting each particle make an individual random two-dimensional (2D) step for each time unit, for a total of 10 000 steps per particle. X and Y displacements per particle and step were obtained by sampling from the Gaussian distributions generated via the Box-Muller method as available in the IDL library. Particle trajectories thus generated were transformed into iMSDs as explained in Sec. III.

III. PARTICLE TRACKING

A. Mean-squared displacement functions

To describe the dynamics of a single particle p, use can be made of its (individual) mean-squared displacement function

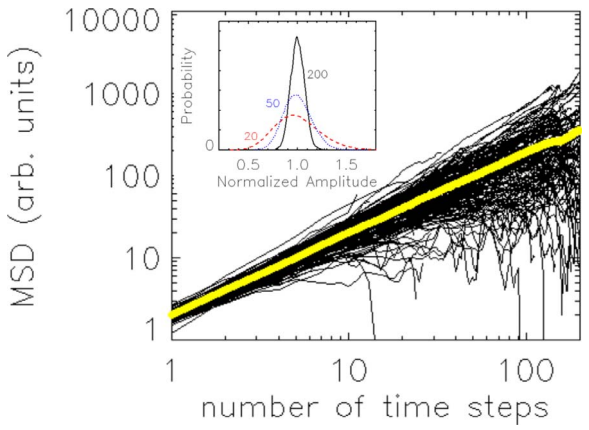

FIG. 1. (Color online) Individual mean-squared displacement functions obtained by simulation for a purely diffusive system. The yellow central line indicates the total MSD obtained by averaging over all particles. Inset: normalized distribution of the iMSD amplitude as a function of the number of contributions to the average: 20 (red dashes), 50 (blue dots), and 200 (black solid line).

$$\Delta r_p^2(\tau) = \sum_{t=1}^{N_t(p,\tau)} \{[x_p(t+\tau) - x_p(t)]^2 + [y_p(t+\tau) - y_p(t)]^2\}/N_t(p,\tau), \quad (1)$$

with $x_p(t)$ and $y_p(t)$ representing the location of the particle at time t and τ as the lag time. Since the localizations are made from video images, both t and τ are expressed in units of the exposure time per image: t_1. Then the number of contributions $N_t(p,\tau)$ is given by $N_t(p,\tau) = (T_p - \tau)/t_1$, with T_p as the duration of the trajectory of particle p. Averaging the iMSD over all particles then produces the total MSD,

$$\Delta r^2(\tau) = \sum_{p=1}^{N_p} N_t(p,\tau)\Delta r_p^2(\tau) / \sum_{p=1}^{N_p} N_t(p,\tau), \quad (2)$$

with N_p as the number of particles. This MSD is commonly used in particle tracking studies. Inspired by the dynamic behaviors displayed in some reference cases [diffusive motion in either (a) elastic or (b) viscous media or (c) ballistic motion], measured MSD functions are often fitted with a power-law function

$$\Delta r^2(\tau) \cong A\left(\frac{\tau}{\tau_{ref}}\right)^{\alpha}, \quad (3)$$

with A as the amplitude at reference time τ_{ref} and α as the power-law exponent (respectively, 0, 1, and 2 for the mentioned cases a, b, and c). For particles embedded in linear viscoelastic materials, fractional exponents can be found, while also transitions in dynamic behavior can manifest themselves at a certain lag time. To account for such cases, use is made of local measures for A and α:

$$A = \Delta r^2(\tau_{ref}), \quad \alpha = \left[\frac{d\ln(\Delta r^2)}{d\ln\tau}\right]_{\tau_{ref}}. \quad (4)$$

In principle, this description can also be applied to the individual MSD functions. An illustration can be found in Fig. 1

for a simulated set of particles in a Newtonian liquid: each of the iMSDs has an amplitude and power-law exponent close to that of the average. This demonstrates that even a single-particle trajectory can already provide a (semi)quantitative measure of the dynamics in the system. It is also seen that the iMSDs display a larger "noise" in A and α at longer lag times. This is a purely statistical effect, due to the random nature of the individual displacements, combined with the decreasing number of contributions $N_t(p,\tau)$ from which the averages are calculated. Figure 1 thus shows both the utility of the iMSD and the potential limitations on its use.

B. Segmentation

In the analysis of iMSD functions, the relation between track length and noise level may need to be taken into account, especially when making statistical comparisons. One approach is to consider only (fragments of) trajectories that contain the same number of time steps. This number (N) should be taken small enough to keep the fraction of lost (i.e., too short) trajectories low and large enough to keep the noise level acceptable. The iMSD of such a fragment is then defined as

$$[\Delta r_p^2]_N(\tau) = \sum_{t=1}^{N-\tau/t_1} \{[x_p(t+\tau)-x_p(t)]^2 + [y_p(t+\tau)-y_p(t)]^2\}/\left(N-\frac{\tau}{t_1}\right), \tag{5}$$

which has N-1 contributions at $\tau=t_1$, N-2 at $\tau=2t_1$, etc. In the remainder of this paper, our analysis will mainly be focused on the amplitude (A_p) of this iMSD for $N=50$ and $\tau=t_1$:

$$A_p \equiv [\Delta r_p^2]_{50}(t_1). \tag{6}$$

C. Spatial and time dependences

The segmentation of trajectories into successive blocks of duration $50^* t_1$ also allows considering A_p as a function of time:

$$A_p(t') = \{A_p(t_1'), A_p(t_2'), A_p(t_3'), \ldots\}, \tag{7}$$

with

$$t_i' = 50\left(i-\tfrac{1}{2}\right)t_1 + t_0' \tag{8}$$

as a new (coarse) time grid. Here t_0' represents the real time at which the trajectory of particle p started. By adding this time, the $A_p(t')$ functions are again synchronized for the different particles so that all of them can be mapped onto a unique real-time grid t' (from now on designated as t for notational convenience). In Fig. 2, an illustration is given of how $A_p(t)$ could look for two hypothetical particles (mimicked by computer simulation). The lower black curve represents a Brownian particle dispersed in a homogeneous liquid with constant viscosity; here the temporal variation in A is purely due to statistical fluctuations. In contrast, the upper red curve corresponds to a particle which transfers to an environment with a higher viscosity. Now a decreasing trend is superimposed onto the fluctuating signal.

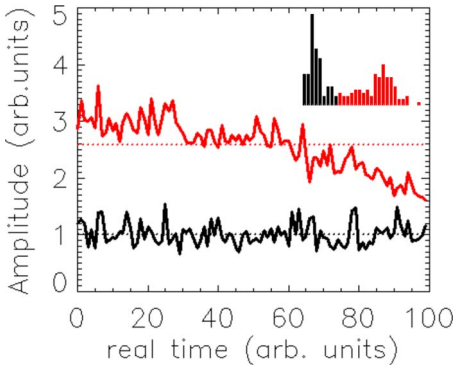

FIG. 2. (Color online) Illustration of two exemplary behaviors of the iMSD amplitude A_p of particle p as a function of real time. Dotted lines show the average over the 100 observations. The inset shows the corresponding histograms of A_p values.

Besides a real time, also a location can be assigned to A, as evident from the fact that each particle p is localized (as a function of time) by the tracking procedure. Considering all particles p present at the same time t_i, the position dependence of A_{t_i} at that time is sampled at the locations (x_p, y_p):

$$A_{t_i}(\underline{r}) = \{A_{p1}(x_{p1},y_{p1}), A_{p2}(x_{p2},y_{p2}), \ldots\}. \tag{9}$$

Following this approach, the collection of all particle trajectories can be cast into a two dimensional matrix, of A values as a function of particle index (columns) and real-time index (rows). Analysis within a row then allows to compare A-values for the same particle at different times [notation: $A_p(t)$], while analysis within a column allows to compare A values for different particles observed at the same time [notation: $A_t(p)$]. This is also illustrated in Fig. 3.

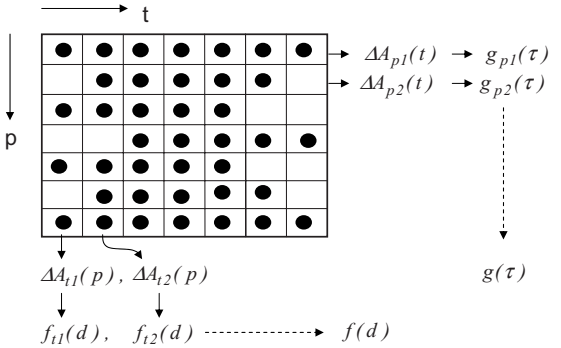

FIG. 3. Schematic illustration of our analysis of iMSD amplitudes. P labels individual particles (and their positions), while t is the index of a time segment in a chronological series. Filled circles indicate for which matrix elements (p,t) a contribution to A exists. Analysis of the rows allows studying fluctuations of A over time via autocorrelation functions $g(\tau)$ or via variances. Analysis of the columns allows quantifying spatial variations in A via cross correlations $f(d)$ or via variances.

D. Time autocorrelation function

Temporal variations in the iMSD amplitude of a given particle can occur if the particle is transferred into a mechanically different environment. One way to study such changes in A_p over time is to calculate its time autocorrelation function. Defining first the temporal fluctuation $\Delta A_p(t)$ of an individual particle p as

$$\Delta A_p(t) \equiv A_p(t) - \langle A_p \rangle_t, \tag{10}$$

with $\langle A_p \rangle_t$ as the time average,

$$\langle A_p \rangle_t = \sum_{t=1}^{N_t(p)} A_p(t)/N_t(p), \tag{11}$$

and $N_t(p)$ as the number of contributions (i.e., the number of elements in row p where A exists); the autocorrelation function of $A_p(t)$ is given by

$$g_p(\tau) = \frac{1}{N_t(p,\tau)} \sum_{t=1}^{N_t(p,\tau)} \Delta A_p(t)\Delta A_p(t+\tau) / \frac{1}{N_t(p)} \sum_{t=1}^{N_t(p)} [\Delta A_p(t)]^2, \tag{12}$$

with $N_t(p,\tau) = (T_p - \tau)/\tau_1$, i.e., as before but now with τ in units of $\tau_1 = 50t_1$. Note that $g_p(\tau)$ is normalized per particle. Obtaining a time autocorrelation function with an acceptable noise level requires a very large number of contributions. If this criterion is not met for the individual functions $g_p(\tau)$ then it may still be possible to obtain an autocorrelation function with an acceptable signal-to-noise ratio (S/N) by averaging over all particles:

$$g(\tau) = \sum_{p=1}^{N_p} N_t(p,\tau) g_p(\tau) / \sum_{p=1}^{N_p} N_t(p,\tau). \tag{13}$$

This total autocorrelation function $g(\tau)$ will be analyzed in Sec. IV.

E. Spatial cross correlation function

Spatial variations in A can be expected in materials where the mechanical properties and/or driving forces depend on location. Then having many probe particles spread out over the material allows sampling of the spatial distribution of these properties. To account for possible temporal variations (i.e., A not only depending on location but also on time), spatial distributions of A will only be considered for particles present at the same time. One way to analyze these is to calculate a spatial correlation function. For this we first define the local deviation ΔA_t (associated with particle p) as

$$\Delta A_t(p) = A_t(p) - \langle A_t \rangle_p, \tag{14}$$

with $\langle A_t \rangle_p$ as the ensemble average,

$$\langle A_t \rangle_p = \sum_{p=1}^{N_p(t)} A_t(p)/N_p(t), \tag{15}$$

and $N_p(t)$ as the number of contributions (i.e., the number of elements in column t where A exists). Then using the coupling between a particle's index p and its position $\underline{r}$, the distance d_{pq} between the centers of two particles p and q is calculated and subsequently binned onto an array $d_i = id_1$, with d_1 as the chosen unit distance. Defining C_{t,d_i} as the collection of all $N_{C_{t,d_i}}$ particle pairs (p,q) for which $d_i \leq d_{pq} < d_{i+1}$ at time t, we then calculate the intermediate function

$$X_t(d_i) = \sum_{p,q \in C_{t,d_i}}^{N_{C_{t,d_i}}} \Delta A_t(p)\Delta A_t(q)/N_{C_{t,d_i}}, \tag{16}$$

which is then used to calculate the (normalized) spatial correlation function at time t,

$$f_t(d_i) = X_t(d_i)/X_t(d_i = 0). \tag{17}$$

Finally, averaging over all time segments t and generalizing for all d_i then gives the total spatial (auto and cross) correlation function

$$f(d) = \sum_{t=1}^{T/\tau_1} N_{C_{t,d_i}} f_t(d)/N_{C_{t,d_i}}. \tag{18}$$

This function is suited for revealing the presence or absence of a spatial correlation length for A and will be analyzed in Sec. IV.

F. Time variance

While correlation functions can provide detailed information about characteristic time or length scales at which a quantity (such as A) shows a change, they also require a huge number of observations to achieve a good S/N ratio. In cases where less data are available, one can still use (normalized) variances to quantify heterogeneity in the distribution of A. Using the definition Eq. (10), the variance in A_p of a particle p over time is given by

$$var^{time}(A_p) = \frac{1}{N_t(p) - 1} \sum_{t=1}^{N_t(p)} [\Delta A_p(t)]^2 \tag{19}$$

and transformed into a relative standard deviation with

$$\sigma_{rel}^{time}(A_p) = \sqrt{var^{time}(A_p)}/\langle A_p \rangle_t. \tag{20}$$

The average relative standard deviation corresponding to the entire particle set (i.e., all rows in Fig. 3) can then be formulated as

$$\sigma_{rel}^{time} = \sum_{p=1}^{N_p} [N_t(p) - 1]\sigma_{rel}^{time}(A_p) / \sum_{p=1}^{N_p} [N_t(p) - 1]. \tag{21}$$

It should be noted that the quantity expressed by Eq. (19) [and hence also Eqs. (20) and (21)] may show an increase with the amount of time over which A is observed: the longer the time, the more opportunity is given to the particle to explore all its accessible values of A. For example if the analysis in Fig. 2 would have been restricted to 50 units rather than 100, then the broadest histogram would have been less broad. This aspect will be further considered in Sec. IV.

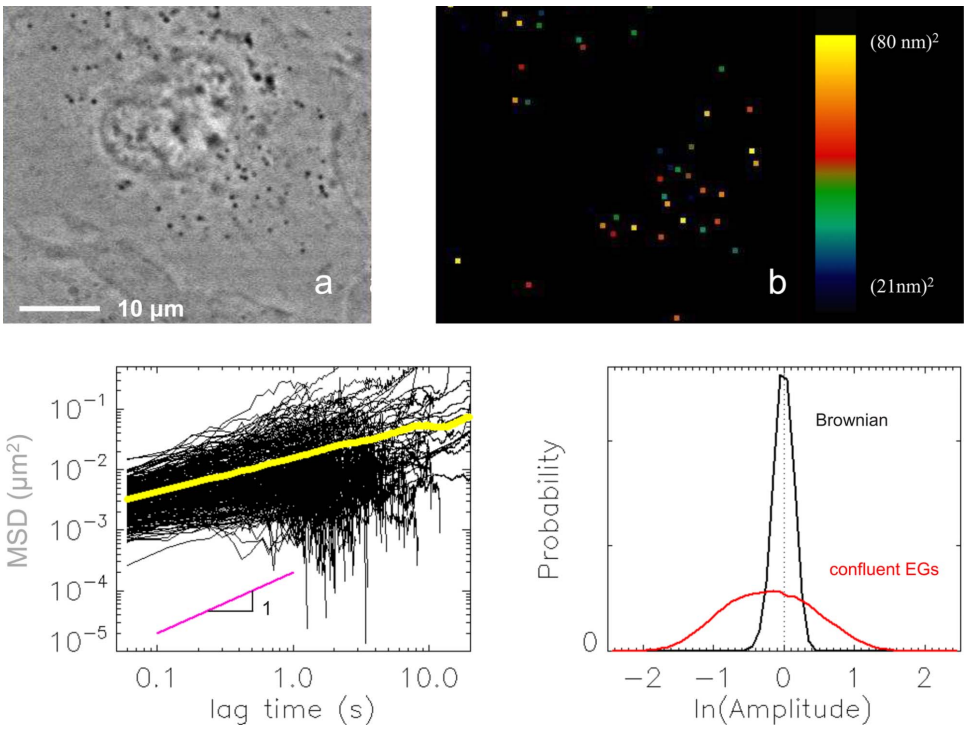

FIG. 4. (Color online) (a) Microscopy image of a Hmec-1 cell containing endogenous granules, visible as dark objects. (b) Reconstruction of (a) in which each particle has been assigned an MSD amplitude, represented via a color scale. (c) Individual and whole cell MSDs as found in a typical experiment. (d) Amplitude histogram for EGs, averaged over all experiments. For comparison, also a histogram for Brownian particles is included. Note the amplitude normalization on the abscissa.

G. Spatial variance

The spatial variance of the amplitude can be calculated in an analogous way as in Sec. III F but now by considering columns instead of rows (Fig. 3). Then the spatial variance and relative standard deviation are defined for each column (i.e., time t) as

$$var^{spatial}(A_t) = \frac{1}{N_p(t) - 1} \sum_{p=1}^{Np(t)} [\Delta A_t(p)]^2 \tag{22}$$

and

$$\sigma_{rel}^{spatial}(A_t) = \sqrt{var^{spatial}(A_t)}/\langle A_t \rangle_p. \tag{23}$$

The total average over all times is then calculated as

$$\sigma_{rel}^{spatial} = \sum_{t=1}^{N_t} [N_p(t) - 1]\sigma_{rel}^{spatial}(A_t)/\sum_{t=1}^{N_t} [N_p(t) - 1]. \tag{24}$$

IV. RESULTS

Figure 4(a) shows a typical microscope image of a Hmec-1 cell loaded with EGs. Tracking these particles over 50 steps of 60 ms, calculating the iMSDs, and representing the amplitudes A hereof [cf. Eq. (6)] with a color scale, results in Fig. 4(b). This map [the graphical equivalent of Eq. (9)] is a representative for a set of 2000 of such images. It is shown that the particles are more or less evenly distributed over the accessible part of the cell interior (which excludes the nucleus and the actin cortex). Importantly, the amplitude A varies appreciably between the particles, up to a factor $\approx$16. This can also be seen from Fig. 4(c), which shows representative iMSD functions [cf. Eq. (1)]. The significance of this heterogeneity, compared to a Brownian particle system (analyzed in the same way), is apparent from the probability distributions in Fig. 4(d).

Figure 4(b) does not show any obvious systematic trends: neither particles close to each other nor particles close to the nucleus seem to display clearly visible correlations. The latter is in contrast with earlier findings [9] for carboxylated latex particles in Swiss 3T3 fibroblasts. For our EGs in quiescent Hmec-1 cells there is clearly strong dynamic heterogeneity, but it does not seem linked to any large scale organization within the cell.

Further (and more quantitative) analyses were performed on the data sets underlying the amplitude maps. Here each data set contained the real time index and for each particle its (x,y) location and its iMSD amplitude A. Although our movies were taken consecutively, time correlations were only calculated within the same movie.

For our correlation analyses, we had to combine the data from all 41 movies to obtain an acceptable accuracy. For the spatial correlations, the number of particle pairs per image is

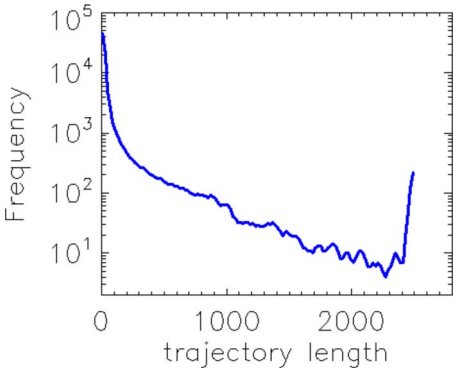

FIG. 5. (Color online) Histogram of trajectory lengths obtained from 41 movies of endogenous granules in a confluent Hmec-1 cell.

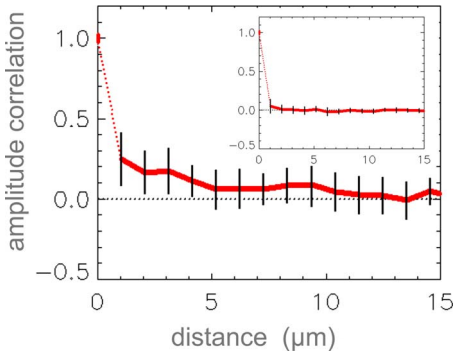

FIG. 6. (Color online) Spatial correlation function [cf. Eq. (18)] for the iMSD amplitude of EGs in Hmec-1 cells. Inset: reference case of polystyrene latex particles in glycerol. Vertical bars indicate standard deviations.

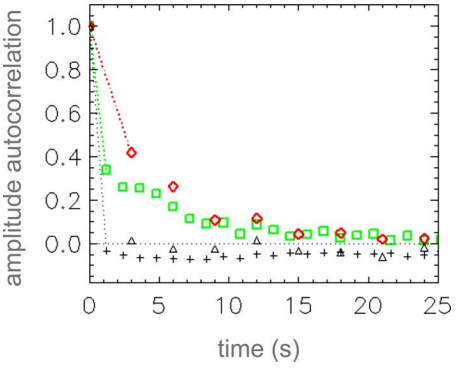

FIG. 7. (Color online) Time autocorrelation function [cf. Eq. (13)] of the iMSD of EGs in Hmec-1 cells. Red diamonds and green squares correspond to segmentation of trajectories into blocks of 50 and 20 units, respectively, of 60 ms. +: latex spheres in glycerol. △: computer simulation for Brownian spheres.

important. On average there were 79 particles per image, giving ≈3000 pairs. For the temporal correlations, both the number of tracks and their duration are important. Figure 5 shows the histogram corresponding to the total data set (before segmentation). Importantly, the number of trajectories longer than 50 steps is high ($>10^4$) and a significant number of very long trajectories is obtained.

The spatial correlation function for A [cf. Eq. (18)] is shown in Fig. 6. The error bars display standard deviations calculated from the spread between the $f(d)$ functions calculated from the 41 individual movies. For comparison we also included the result of the same analysis procedure but now for carboxylated poly(styrene) [PS] latex particles in glycerol (see inset). Probably due to the larger number of particles per image, the noise level is somewhat lower in the latter experiment. The correspondence with the zero level is very good, in line with expectations: for particles showing purely random (i.e., Brownian) motion, correlations between the motion amplitudes of different particles should indeed be absent.

For EGs in Hmec-1 cells, the magnitude of the correlation function lies mostly between 0 and 0.1. Considering that the function is normalized to 1.0, this suggests that correlations are either weak or absent. The slight upturn of the curve for distances below 4 μm might however still be significant. Making a more definitive statement would require more particle pairs in close proximity. In our case interparticle separations of 1 μm were already relatively sparse (2×10^4 contributions), and achieving a sufficient number of contributions at even smaller distances would require a prohibitively large number of movies. Probably for the same reason, Van Citters *et al.* [15] were not able to calculate a reliable D_{rr} for distances smaller than 2 μm. As a last remark on this issue, we note that a fundamental lower limit on the spatial resolution would ultimately be set by the fact that the particles are mobile. In our case, the typical displacement over 50 time steps of 60 ms amounted to ≈40 nm.

In summary, the results in Fig. 6 mainly confirm our expectation [based on inspection of many images such as those in Fig. 4(b)] that clear spatial correlations in iMSD amplitude are absent. This result corresponds well to the findings for TC7 epithelial cells, where a similar conclusion was drawn based on an analysis using two-point microrheology [15].

We now turn to time correlations. Figure 7 shows the iMSD time autocorrelation function (diamonds) as calculated from Eq. (13), averaging over trajectories from all available movies. For comparison, we also calculated the same function based on the same 41 movies but now with trajectories segmented into blocks of 20 steps (squares). For both these calculations on EGs in Hmec-1 cells, we used only trajectories of 1000 or more unit time steps so that at least 20 (respectively, 50) time points were available for calculating the autocorrelation function. That this was an adequate criterion to ensure significant results is illustrated by the correspondence between the two curves.

Moreover we also applied this procedure to particle tracking experiments with latex particles in glycerol and to data sets generated via the Brownian dynamics simulations. In the latter two cases zero correlation is expected for all lag times (except $\tau=0$) since in purely viscous systems the Langevin equation does not contain any memory term that links the current motion of a particle to its previous displacements. The reference data in Fig. 7 confirm the immediate loss of correlation, and the achievement of values very close to zero. The small negative deviation from zero displayed by the latex/glycerol data is attributed to the finite number of contributions to the correlation function.

Returning to the case of EGs in Hmec-1 cells, it is first of all clear that for times >10 s no correlations can be detected. The upturn of the curves for correlation times shorter than ≈10 s suggests that the iMSD amplitude of endogenous granules in Hmec-1 cells takes about 10 s to decorrelate. Clearly this significant difference from the Brownian reference case suggests the presence of some kind of intracellular reorganization at this time scale. Whether this would be cytoskeleton remodeling, (un)binding to cytoskeletal elements, or simply cage rattling, this cannot be stated and requires additional independent measurements.

We further note that while the plotted autocorrelation function indicates the existence of a correlation time, it does not reveal the magnitude of the changes in amplitude variation. To illustrate this multiplying the deviation $\Delta A_p(t)$ given

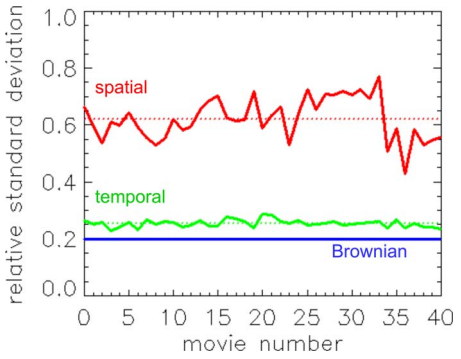

FIG. 8. (Color online) Relative standard deviations in the iMSD amplitude of EGs in Hmec-1 cells, calculated in two different manners. Spatial: cf. Eq. (24). Temporal: cf. Eq. (21). Dotted lines indicate averages over the 41 movies. For Brownian particles in Newtonian liquids, both averages coincide at 0.20.

by Eq. (10) with an arbitrary constant will not change the correlation function given by Eq. (12). So while short-time temporal correlations are present, their quantitative contribution to the MSD amplitude heterogeneity still has to be assessed. Finally we remark that insufficient long trajectories were available to obtain a reliable correlation function for $\tau > 25$ s. However the fact that $g(\tau)$ already reaches near-zero values at $\tau = 25$ s implies that the time needed for a change in average A comparable to the amplitude of the short-time fluctuations ΔA is $\gg 25$ s.

To assess the relative importance of spatial and temporal variations in iMSD amplitude, we now turn to variance analysis. Analyzing distributions for variance does not require the vast amount of data as needed for the correlation functions since only one number has to be calculated (rather than a binned distribution). To illustrate the idea we again consider Fig. 2, with the two hypothetical $A(t)$ profiles. Both profiles show fluctuations, but these are smaller than the difference between the average magnitudes of A. This is also shown by the bar histograms shown in the inset. Besides the average, also the variance is different for the two distributions. This is because upper profile not only fluctuates but also gradually decreases over time.

The comparison in Fig. 2 stands model for an important case: the difference in average iMSD between particles is larger than the variations in iMSD shown by individual particles in the experimental time window (150 s). If this duration were very long, then both particles might explore the same set of accessible iMSD values (assuming the particles remain indistinguishable by nature), and the then resulting amplitude histograms would coincide. However on short time scales each particle explores only part of its "iMSD configuration space." Hence differences in the two variances, (1) over particles (i.e., space) and (2) over time, can reveal the presence of different microenvironments, as far as they are significant over the (150 s) time scale of the experiment.

Let us now consider the iMSD amplitude variations for EGs in Hmec-1 cells displayed in Fig. 8. Clearly, for each of the 41 recorded movies, the temporal variations within the trajectories are significantly smaller than the variations between particles. Moreover the relative standard deviation of the temporal variations is only slightly larger than the expected value of 0.20 ($\sqrt{2/N}$ with $N=50$) for the Brownian displacements. [For a Gaussian distribution $P(\Delta x)$ with variance σ^2, the expected variance of $(\Delta x)^2$ amounts to $2\sigma^4$, giving a relative standard deviation of $\sqrt{2\sigma^4}/\sigma^2$. Then averaging over N samples, this quantity reduces with a factor $1/\sqrt{N}$.] Importantly, this demonstrates that the different EGs in Hmec-1 cells experience different microenvironments.

We also studied the relative standard deviation due to temporal variations in the iMSD of the same particle in more detail. If the relative standard deviation calculated from the time dependence is due to more than stochastic fluctuations alone, which is indeed suggested ($0.26 > 0.20$), then a certain time dependence does exist. In that case, the calculated σ_{rel} should increase with the duration of the trajectory (as explained in Sec. III F). To examine this time dependence for the EGs, we sorted all nonsegmented trajectories according to their length l (see Fig. 5) and computed $\sigma_{rel}(l)$ by averaging over all 41 movies. We found that $\sigma_{rel}(l)$ gradually evolved from 0.20 at a track duration of 10 s to 0.26 for a duration of 150 s. This indicates that at time scales up to 10 s the iMSD changes are rather small indeed and also the increase in temporal heterogeneity over 150 s is still modest. Apparently the time needed for important changes is indeed $\geqslant 150$ s, as was also suggested from the time autocorrelation function.

V. DISCUSSION

A. Implications for particle tracking studies

A method for characterizing spatial and temporal heterogeneity in particle dynamics was applied to endogenous granules in living Hmec-1 cells. We found appreciable local variations in iMSD but no systematic dependence on intracellular location [Fig. 4(b)]. An important implication hereof is that the precise distribution of the probes inside the cytoplasm is not crucial for observing a dynamic behavior that is representative for the whole cell. As long as the number of probes is high enough to sample the distribution of microenvironments, the variations in MSD will be averaged out. This means that it is justified to analyze the response of cells, e.g., to drug treatments via the standard (i.e., ensemble averaging) particle tracking methods, even if the treated and untreated cells (and hence also their intracellular particle distributions) are different.

Also the absence of important transitions in the MSD of single particles, at least for durations up to 150 s (Figs. 7 and 8), has an important implication. It means that individual dynamic behaviors observed in this time window can be considered without an obvious need for trajectory segmentation. In other words, each particle will reflect an individual dynamics, which can be measured and analyzed directly from its MSD-vs-lag time dependence, regardless of trajectory duration. These considerations will be further used in Sec. V B, in which we will analyze distributions of both the amplitude A and the initial exponent α obtained from individual trajectories.

B. Application of individual trajectory analysis

In this section we follow up on the finding that the heterogeneity in the iMSDs of our Hmec-1 cells is primarily

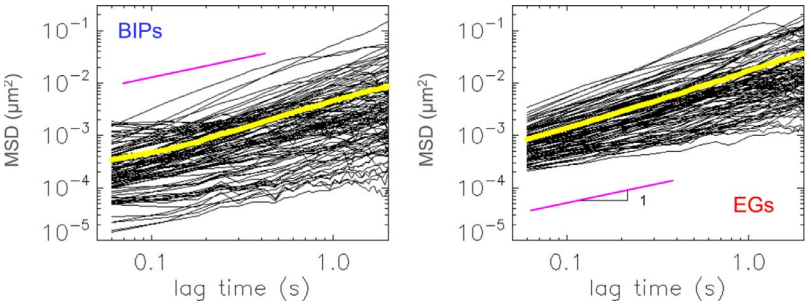

FIG. 9. (Color online) Representative set of 100 iMSD functions [based on trajectory segments cf. Eq. (5)] for BIPs (left) and EGs (right) in Hmec-1 cells. Average MSDs [cf. Eq. (2)] are shown in yellow. Solid magenta lines indicate a power-law exponent of 1.

due to differences between (the local environments of) particles. In other words, both the intracellular location of the particle and the integration time used for measuring the iMSD are relatively unimportant. Hence it is sufficient to consider lumped distributions of iMSDs. Besides EGs we here also consider BIPs as described in Sec II B. For these particles, less data could be obtained by particle tracking, due to phototoxic effects of the laser illumination (showing within minutes of exposure). Yet, graphs similar to Figs. 4 and 8 suggested that also for these probes, the spatial heterogeneity was dominant.

In Fig. 9 we show typical sets of iMSDs (based on segmented trajectories) of BIPs and EGs in (here nonconfluent) Hmec-1 cells. Similar to Fig. 4, broad amplitude distributions are found, for the BIPs even more than for the EGs. It is also apparent for both probe types that the (log-log) slopes show variations from particle to particle. In addition, some iMSDs appear noisy. This applies mostly to the BIPs for which the particle displacements are sometimes rather small.

Fitting power laws to the first three points of the iMSD functions, we obtained for each trajectory segment an amplitude A and a power-law exponent α, which we then collected into histograms. To compare histograms obtained for different probe/matrix combinations, they have to be brought onto a common (i.e., reduced) scale. For the dimensionless α this was not needed. For the amplitude A this was achieved by subtracting $\langle \ln(A) \rangle$ from the distributed values of $\ln(A)$. The results shown in Fig. 10 are striking. First, the amplitude histograms do not resemble a simple lognormal distribution as found in [15,36–38]. This applies most strongly to BIPs, for which it could already be seen from Fig. 9 that more than one type of particle dynamics occurs. For EGs the correspondence is better.

Also the power-law exponent α shows a remarkably broad distribution. It is now apparent that while the ensemble averaged MSDs for BIPs and EGs are close to simple behaviors (the average α being close to 0 and 1, respectively), in fact a significant variety in the dynamic behavior occurs for both probes. This holds the most strongly for the EGs, where it is suggested that besides diffusive, both subdiffusive and superdiffusive behaviors occur. A biophysical interpretation of the differences between EGs and BIPs will be given elsewhere [39,40].

We now consider some statistical aspects in the analysis of histograms such as Figs. 10(a) and 10(b). First of all we remark that dividing trajectories into segments of standard length is recommended when comparing such histograms. One reason for this is that it standardizes the broadening that takes place due to the finite trajectory lengths. This point is most clearly illustrated by the distributions obtained from the Brownian dynamics simulation. Here each particle had been given the same diffusivity, implying that the expectation values for A and α were exactly the same. Yet distributions are observed. For longer trajectory segments, these distributions become sharper. For our EGs in Hmec-1 cells studied with our camera, 50 steps per segment was an optimal choice. Choosing $N>50$ would have meant exclusion of a substantial fraction of the shortest trajectories from the analysis (see Fig. 5), possibly giving biased results, since in systems with heterogeneous dynamics the "faster" particles generally have shorter trajectories [41]. A second reason for segmentation into standard blocks is that this can compensate for bias due to the different frequencies at which "slow" and "fast" particles leave and re-enter the focal plane of the microscope (and hence create "new" trajectories [34]).

We attribute the occurrence of negative values of α for BIPs in Fig. 10(b) to the statistical broadening around an average α that is close to 0. To corroborate this, we reanalyzed the BIPs trajectories after segmentation into blocks of 200 steps. As can be seen from Fig. 10(b), the occurrence of negative values has indeed become smaller. Following the same logic, a similar question could be posed about the sig-

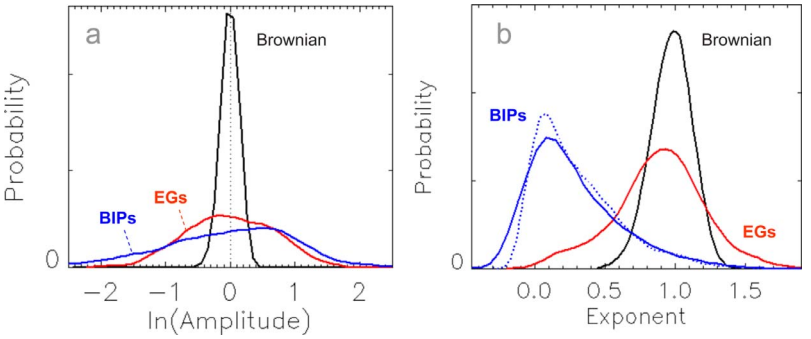

FIG. 10. (Color online) Probability distributions for the logarithm of amplitude ($\ln A$) and power-law exponent (α) measured at $\tau \approx 0.1$ s for two probe particles (EGs and BIPs) in individual Hmec-1 cells. For comparison, also the case of monodisperse particles in a Newtonian liquid is included. Distributions for $\ln A$ have been centered on zero. For BIPs the distribution of α is also shown for segmentation into blocks of 200 steps (dotted line).

nificance of the apparently superdiffusive behavior ($\alpha > 1$) displayed by a fraction of the EGs. However, in this case a comparison can be made with the curve for the Brownian system, for which the average α is approximately the same. For the latter system, the chance of finding $\alpha > 1.4$ for an iMSD based on 50 time steps is very small. Yet for EGs a substantial fraction of trajectories with $\alpha > 1.4$ is still observed. This indicates that for EGs there exist superdiffusive behaviors, which are however hidden under an apparently simple diffusive overall MSD. This finding is qualitatively in line with the results of [13,42].

C. Comparison with other particle tracking methods

The analysis method presented in this paper provides a straightforward extension of 1PMR. As such it also shares advantages and drawbacks of 1PMR. Depending on the selected probes and the embedding material of interest, the MSD function can reflect viscoelastic properties and/or probe-matrix interactions. In "materials" such as living cells, there may also be an additional contribution to the particle dynamics by ATP-dependent driving forces. Consequently, different (combinations of) properties can be studied with 1PMR. Knowledge of the chemistry between the probe and the matrix and/or the ability to eliminate nonthermal driving forces can then simplify interpretation. In this respect, living cells provide the biggest opportunities and challenges. This is however not limited to 1PMR. Also in 2PMR the particle dynamics can no longer be related directly to the intracellular rheology if nonthermal driving forces are acting.

What makes 2PMR unique is that it does not suffer from a lack of knowledge on the probe-matrix interactions due to the fundamentally different measurement principle. In 2PMR one measures the correlated vectorial displacements of two particles caused by the transmission of strain through the effective medium in between. For interparticle distances large compared to the typical size of a microenvironment, these correlations become insensitive to the microenvironments of the individual probes. Consequently, even in case of local probe-matrix interactions (such as adhesion or repulsion, which can cause changes in the local microstructure), the measurement will reflect properties of the medium that have been averaged over large length scales. While this aspect makes 2PMR more comparable to macroscopic rheology, it also makes 2PMR less suited for studying spatial heterogeneities. For example it may be found that $D_{rr}(r)$ does not scale anymore as $\sim 1/r$, but then other methods will be needed for further inspection of heterogeneities.

Our method is hence complementary to both 1PMR and 2PMR in their standard application, neither of which reveals detailed information about spatial heterogeneity. Illustrations of spatial heterogeneity, both quantitatively (i.e., iMSD amplitude) and qualitatively (i.e., both subdiffusivity and superdiffusivity) were given in this paper. In principle this analysis could also be taken further using a software to detect and analyze subgroups of particles separately, based on their iMSD. Such an approach was already successfully applied to materials containing mechanically distinct (micro)phases [24].

A similar argument holds for temporal heterogeneity. Standard applications of 1PMR and 2PMR are not suited for detecting transitions from one dynamic behavior to the other by the same particle. However with trajectory segmentation as in Eq. (5) and variance analysis as in Eq. (21), it should be possible to detect for example the occurrence of intermittent dynamics [19,43] even if this occurs for only a small fraction of the particles.

VI. CONCLUSIONS AND OUTLOOK

In this paper, we addressed spatiotemporal heterogeneity in the dynamics of endogenous lipid granules in living Hmec-1 cells. Careful analysis of large sets of individual particle MSDs, considering distributions over time as well as over particle populations, allowed us to conclude that at the time scales pertinent to our experiments (150 s), particles can be distinguished according to their dynamic behavior. This allowed straightforward interpretation of distributions for the amplitude and power-law exponent. It thus became clear that not only the motion amplitude but also the type of dynamics showed considerable heterogeneity.

The implication hereof for obtaining a reliable ensemble averaged MSD, is that many particles per cell and/or trajectories consisting of many steps are needed. If (like in our case) spatial correlations between the different particles are absent, then the intracellular distribution of the particles will not have to be taken into account. The important implication of this outcome is that ensemble averaged MSDs measured in cells of the same type but not the very same cell can still be meaningfully compared. This opens up the road to diagnosing living cells (e.g., before and after pharmacological interventions) via their MSD even if the treated and untreated cells are not the same.

Finally we conclude that the statistical tools that were used to analyze spatiotemporal heterogeneity should be equally applicable to a variety of other materials in which such heterogeneities occur. Measurements of correlation distances and times will require very large data sets. But even if these are not available, a straightforward analysis of relative variances could already provide a quick "fingerprint" of heterogeneity.

ACKNOWLEDGMENTS

This research was carried out in the "Cell stress" Strategic Research Orientation of the MESA+ institute for nanotechnology. We thank Dirk van den Ende for stimulating discussions on particle tracking.

[1] T. A. Waigh, Rep. Prog. Phys. **68**, 685 (2005).
[2] D. Weihs, T. G. Mason, and M. A. Teitell, Biophys. J. **91**, 4296 (2006).
[3] T. G. Mason, Rheol. Acta **39**, 371 (2000).
[4] S. R. Heidemann and D. Wirtz, Trends Cell Biol. **14**, 160 (2004).
[5] T. P. Kole, Y. Tseng, I. Jiang, J. L. Katz, and D. Wirtz, Mol. Biol. Cell **16**, 328 (2005).
[6] P. Panorchan, J. S. H. Lee, B. R. Daniels, T. P. Kole, Y. Tseng, and D. Wirtz, *Cell Mechanics* (Academic (Elsevier), San Diego, 2007), Vol. 83, p. 115.
[7] P. Panorchan, J. S. H. Lee, T. P. Kole, Y. Tseng, and D. Wirtz, Biophys. J. **91**, 3499 (2006).
[8] Y. Tseng, T. P. Kole, S. H. J. Lee, and D. Wirtz, Curr. Opin. Colloid Interface Sci. **7**, 210 (2002).
[9] Y. Tseng, T. P. Kole, and D. Wirtz, Biophys. J. **83**, 3162 (2002).
[10] S. Yamada, D. Wirtz, and S. C. Kuo, Biophys. J. **78**, 1736 (2000).
[11] J. C. Crocker and B. D. Hoffman, in Ref. [6], p. 141.
[12] B. D. Hoffman, G. Massiera, K. M. Van Citters, and J. C. Crocker, Proc. Natl. Acad. Sci. U.S.A. **103**, 10259 (2006).
[13] A. W. C. Lau, B. D. Hoffman, A. Davies, J. C. Crocker, and T. C. Lubensky, Phys. Rev. Lett. **91**, 198101 (2003).
[14] G. Massiera, K. M. Van Citters, P. L. Biancaniello, and J. C. Crocker, Biophys. J. **93**, 3703 (2007).
[15] K. M. Van Citters, B. D. Hoffman, G. Massiera, and J. C. Crocker, Biophys. J. **91**, 3946 (2006).
[16] C. Wilhelm, Phys. Rev. Lett. **101**, 028101 (2008).
[17] C. Wilhelm, A. Cebers, J. C. Bacri, and F. Gazeau, Eur. Biophys. J. **32**, 655 (2003).
[18] P. Bursac, B. Fabry, X. Trepat, G. Lenormand, J. P. Butler, N. Wang, J. J. Fredberg, and S. S. An, Biochem. Biophys. Res. Commun. **355**, 324 (2007).
[19] P. Bursac, G. Lenormand, B. Fabry, M. Oliver, D. A. Weitz, V. Viasnoff, J. P. Butler, and J. J. Fredberg, Nature Mater. **4**, 557 (2005).
[20] J. L. McGrath, J. H. Hartwig, and S. C. Kuo, Biophys. J. **79**, 3258 (2000).
[21] M. T. Valentine, Z. E. Perlman, M. L. Gardel, J. H. Shin, P. Matsudaira, T. J. Mitchison, and D. A. Weitz, Biophys. J. **86**, 4004 (2004).
[22] D. Mizuno, C. Tardin, C. F. Schmidt, and F. C. MacKintosh, Science **315**, 370 (2007).
[23] J. C. Crocker, M. T. Valentine, E. R. Weeks, T. Gisler, P. D. Kaplan, A. G. Yodh, and D. A. Weitz, Phys. Rev. Lett. **85**, 888 (2000).
[24] M. T. Valentine, P. D. Kaplan, D. Thota, J. C. Crocker, T. Gisler, R. K. Prud'homme, M. Beck, and D. A. Weitz, Phys. Rev. E **64**, 061506 (2001).
[25] D. Weihs, M. A. Teitell, and T. G. Mason, Microfluid. Nanofluid. **3**, 227 (2007).
[26] C. Oelschlaeger, N. Willenbacher, and S. Neser, Prog. Colloid Polym. Sci. **134**, 74 (2008).
[27] F. K. Oppong and J. R. de Bruyn, J. Non-Newtonian Fluid Mech. **142**, 104 (2007).
[28] F. K. Oppong, L. Rubatat, B. J. Frisken, A. E. Bailey, and J. R. de Bruyn, Phys. Rev. E **73**, 041405 (2006).
[29] J. Y. Xu, Y. Tseng, C. J. Carriere, and D. Wirtz, Biomacromolecules **3**, 92 (2002).
[30] W. K. Kegel and A. van Blaaderen, Science **287**, 290 (2000).
[31] T. Moschakis, B. S. Murray, and E. Dickinson, Langmuir **22**, 4710 (2006).
[32] J. H. Dangaria and P. J. Butler, Am. J. Physiol.: Cell Physiol. **293**, C1568 (2007).
[33] S. S. Rogers, T. A. Waigh, and J. R. Lu, Biophys. J. **94**, 3313 (2008).
[34] http://www.physics.emory.edu/~weeks/idl/
[35] J. C. Crocker and D. G. Grier, J. Colloid Interface Sci. **179**, 298 (1996).
[36] B. Fabry, G. N. Maksym, J. P. Butler, M. Glogauer, D. Navajas, N. A. Taback, E. J. Millet, and J. J. Fredberg, Phys. Rev. E **68**, 041914 (2003).
[37] B. Fabry, G. N. Maksym, S. A. Shore, P. E. Moore, R. A. Panettieri, J. P. Butler, and J. J. Fredberg, J. Appl. Physiol. **91**, 986 (2001).
[38] N. Desprat, A. Richert, J. Simeon, and A. Asnacios, Biophys. J. **88**, 2224 (2005).
[39] S. A. Vanapalli, Y. Li, F. Mugele, and M. H. G. Duits (unpublished).
[40] Y. Li, S. A. Vanapalli, F. Mugele, M. H. G. Duits (unpublished).
[41] T. Savin and P. S. Doyle, Phys. Rev. E **76**, 021501 (2007).
[42] A. Caspi, R. Granek, and M. Elbaum, Phys. Rev. Lett. **85**, 5655 (2000).
[43] Z. Bomzon, M. M. Knight, D. L. Bader, and E. Kimmel, J. Biomech. Eng. **128**, 674 (2006).